

Viscous flow through a finite-width slit: Boundary conditions and dissipation

Daniil Asafov,¹ Valentin Kachorovskii,² Konstantin Tikhonov,³ and Gu Zhang⁴

¹*National Research University Higher School of Economics, 101000 Moscow, Russia*

²*Ioffe Institute, 194021 St. Petersburg, Russia*

³*Skolkovo Institute of Science and Technology, Moscow, 121205, Russia*

⁴*Beijing Academy of Quantum Information Sciences, Beijing 100193, China*

(Dated: August 8, 2022)

We study the electronic transport through a finite-size slit in a barrier in a two-dimensional sample in the hydrodynamic regime. We assume a negligible disorder-induced Ohmic resistance, so that dissipation is purely viscosity-induced. We find that the only solution to the Stokes equation in this geometry, which yields a finite dissipation at finite resistance (and, hence, is not self-contradictory), is the one that fulfills both the no-stress and no-slip boundary conditions simultaneously. As a remarkable consequence, the obtained velocity profile satisfies the so-called “partial-slip” (Maxwell) boundary condition for any value of the slip length λ , which drops out from all final results. We also calculate the electronic temperature profile for the small and large heat conductivity, and find asymmetric (with respect to the barrier) temperature patterns in the former case.

I. INTRODUCTION

Rapid developments of nanotechnology in recent years led to fabrication of ultra-clean ballistic systems, where disorder scattering is negligible. As a result, we are witnessing the boom of interest in electronic transport in the viscous hydrodynamic regime, where electron motion is governed by the Stokes equation. In the last decade, various exotic and unique features of electronic hydrodynamics were predicted theoretically (for review, see Refs. [1–4]). These include super-ballistic charge transport (with conductance higher than the ballistic conductance) through a slit [5], as well as an abrupt viscosity-induced jump in the electric potential at the metallic contacts [6]. These predictions, which greatly contrast with common knowledge on transport in disordered systems, have inspired a great amount of recent experimental investigations [7–34]. To date, most of these studies focus on the electric properties including the electric potential and the velocity profiles. Most recently, the fast development of the SQUID-on-tip (tSOT) [34–42] and the cryogenic quantum magnetometry [24] techniques has enabled another intriguing direction of research—the high-resolution detection of the temperature distribution in the hydrodynamic regime.

On the theoretical side, solutions in the hydrodynamic regime rely heavily on the choice of boundary conditions. There are two widely accepted boundary conditions: the no-slip, with zero velocity along the boundary

$$\text{no-slip: } v_{\parallel}|_{\text{boundary}} = 0, \quad (1)$$

and no-stress, with zero shear stress at the boundary

$$\text{no-stress: } \partial_{r_{\perp}} v_{\parallel}|_{\text{boundary}} = 0, \quad (2)$$

conditions. Here r_{\perp} and v_{\parallel} refer to the direction perpendicular to the boundary and the velocity along the boundary, respectively. It was proposed [43, 44] that these two boundary conditions can in general be unified by the “partial-slip” (Maxwell [45]) boundary condition

$$v_{\parallel}|_{\text{boundary}} = \lambda \partial_{r_{\perp}} v_{\parallel}|_{\text{boundary}}. \quad (3)$$

Physically, λ can be interpreted as the slip length for particles at the boundary. Typically, solutions of the Stokes equation with boundary conditions Eqs. (1) and (2) result in distinct velocity profiles with different characteristics. A prime example is the Poiseuille flow which shows finite and zero resistance for no-slip and no-stress conditions, respectively. This implies that generically, the system-specific boundary conditions can be probed experimentally. Recently, there have also been theoretical debates on the validity of these two boundary conditions in graphene [5, 43, 46]. It worth also noting that the no-slip (1) and the no-stress (2) boundary conditions are frequently associated with the limits $\lambda \rightarrow 0$ and $\lambda \rightarrow \infty$ in Eq. (3), respectively. However, as we are going to show in this paper, this natural distinction may fail, since both sides of Eq. (3) may be zero.

More precisely, in this paper, we demonstrate that, surprisingly, the no-stress and no-slip boundary conditions can co-exist, i.e., can be satisfied simultaneously in some specific geometries. This, in turn, means that the Maxwell boundary condition, Eq. (3), is satisfied for any λ , and, consequently, the velocity profile does not depend on λ .

We analyze the velocity and temperature profiles in a two-dimensional (2D) sample where two semi-infinite planes are separated by the infinite barrier with a finite-size slit, as shown in Fig. 1. Such a structure can be easily realized experimentally by using specific gate configuration. Electronic flow through similar systems and associated dissipation patterns have been studied theoretically long time ago in Ref. [47] for disorder-dominated regime ignoring viscous effects. More recently, this system has been addressed in the context of viscous electronic hydrodynamics Refs. [5, 44, 48–50].

We neglect the disorder-induced sample resistance, and investigate the viscosity-controlled hydrodynamic veloc-

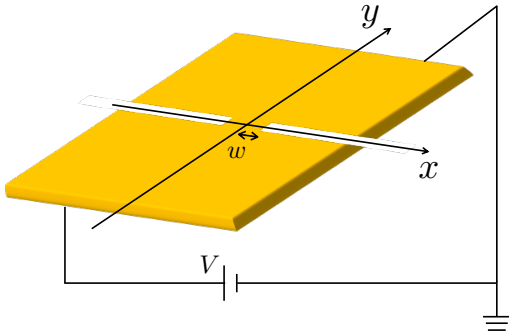


FIG. 1. Schematics of the two-dimensional sample we consider. Charge and heat transfers are only allowed through a slit located at $y = 0$ inside the segment from $x = -w$ to $x = w$. The rest of the sample at $y = 0$ constitutes the impenetrable barrier (white region). The barrier thickness is infinitesimal in the y direction. The sample is biased by a voltage V between the $y < 0$ and the $y > 0$ half-planes.

ity profile for fixed voltage drop across the system, i.e., between lines $y = -\infty$ and $y = \infty$. We show that this condition together with any standard boundary conditions, say “no-slip” or “no-stress”, is not sufficient to uniquely find velocity profile. In particular, we find that the “no-stress” boundary condition allows for a family of solutions with a finite total current through the slit [see below solution Eq. (35)]. We demonstrate that the solution can be uniquely determined only after enforcing the total dissipation in the whole system to be finite. Remarkably, the solution corresponding to finite dissipation satisfies simultaneously both the “no-slip” and “no-stress” boundary conditions, and, consequently, satisfy the partial-slip boundary condition, Eq. (3), for any value of λ . This is our key result.

The system under study was discussed previously. In Ref. [48], a solution was found, which satisfies the no-stress condition (2), but does not satisfy the no-slip condition (1). As we demonstrate below, this solution yields a divergent total dissipation and, therefore, is nonphysical. The solution we obtained is also not captured by the point-contact approximation used in Ref. [44]. Although the resistance in our solution equals to the “superballistic” resistance reported in Ref. [5] for the no-slip boundary conditions, the velocity profile in the whole plane was not reported in Ref. [5] and the fact that this solution also satisfies the no-stress condition (2) was not mentioned there.

We also solve the heat balance equation and find temperature distribution. We demonstrate that the temperature is strongly increased near the slit endpoints. The shape of overheated regions depends on heat conductivity. For small heat conductivity, the heat transfer is dominated by convection and these regions are strongly asymmetric with respect to the barrier separating the

two half-planes. In the limit of zero heat conductivity, the temperature diverges at the slit endpoints. With increasing the heat conductivity, the overheating decreases and the shape of the hot areas becomes more and more symmetric.

The rest of the paper is organized as follows. In Sec. II, we describe the model and hydrodynamic approach. In Sec. III, we analyze the velocity profiles in light of the finite-dissipation requirement. In Sec. IV, we discuss the general approach for the case of finite slip length. The electronic temperature profile is found in Sec. V. Finally, we summarize our results in Sec. VI. Technical details are presented in Appendixes.

II. THE MODEL

The model we consider consists of two clean homogeneous semi-infinite planes connected by a finite-width slit placed at the x axis ($y = 0$ and $-w < x < w$), as shown in Fig. 1. Particle and energy transmission between these two planes is allowed only through this slit, but forbidden everywhere else. We consider a viscous flow through the slit, which is generically described by the Stokes equation

$$\eta \nabla^2 \mathbf{v} = Ne \nabla \phi(\mathbf{r}). \quad (4)$$

Here, η denotes the viscosity coefficients, N is the particle density, $\mathbf{v} = (v_x, v_y)$ is the fluid velocity vector, and ϕ is the electric potential, satisfying the Laplace equation $\Delta \phi = 0$.

Equation (4) describes a sample with a negligible Ohmic resistance, where the driving field $-\nabla \phi$ is balanced by the viscous force. From the energy conservation perspective, the driving power equals the dissipation due to viscosity, with the corresponding power density

$$P(x, y) = \eta \left[\left(\frac{\partial v_x}{\partial x} - \frac{\partial v_y}{\partial y} \right)^2 + \left(\frac{\partial v_y}{\partial x} + \frac{\partial v_x}{\partial y} \right)^2 \right]. \quad (5)$$

We note that, once the velocity and/or the stress tensor at the wall are zero, there is no boundary contribution to the total energy change in the system [6].

The non-equilibrium driving is included via the application of a voltage bias V between the lower ($y < 0$) and the upper ($y > 0$) half-planes. At positions far away from the slit, $r \equiv \sqrt{x^2 + y^2} \gg w$, the electric potential is given by

$$\phi(\mathbf{r})|_{r \rightarrow \infty, y > 0} = 0, \quad \phi(\mathbf{r})|_{r \rightarrow \infty, y < 0} = V \quad (6)$$

in the two half-planes.

Equation (4) has been already considered for the charge transport through a point contact [44] or a finite-size slit [5, 48]. After the introduction of the vorticity

$$\omega = [\nabla \times \mathbf{v}] \cdot \hat{n}, \quad (7)$$

the Stokes equation (4) becomes

$$[\hat{n} \times \nabla \omega(\mathbf{r})] = \frac{Ne}{\eta} \nabla \phi(\mathbf{r}), \quad (8)$$

where \hat{n} is the unit vector perpendicular to the 2D plane. Taking the curl of Eq. (8), one finds that the vorticity satisfies the Laplace equation: $\Delta \omega = 0$.

Vorticity $\omega(\mathbf{r})$ and electric potential $\phi(\mathbf{r})$ satisfy the Cauchy-Riemann conditions in a complex plane with its real and imaginary axes directed along x and y , correspondingly. This means that the combination of these two functions

$$f(z) = -\frac{Ne}{\eta} \phi(\mathbf{r}) + i\omega(\mathbf{r}) \quad (9)$$

is a holomorphic function, with $z = x + iy$. In the no-stress case, the vorticity vanishes at the walls.

We thus have to find a complex function, holomorphic in the upper half-plane, which has a prescribed imaginary part (vorticity) on some pieces of the boundary and real part (electric potential) on other pieces of the boundary. Some particular solutions to this problem are delivered by the Keldysh-Sedov theorem[51], see Appendix A for details. The function $f(z)$ can be found in the closed form [48]:

$$f(z) = \frac{NeV}{2\eta} \left[-1 + \frac{z}{\sqrt{z^2 - w^2}} \right], \quad (10)$$

where the cuts defining the square root $\sqrt{z^2 - w^2}$ run along the screen. Note that with this convention,

$$\overline{\sqrt{z^2 - w^2}} = -\sqrt{\bar{z}^2 - w^2}$$

(throughout the paper, the bar denotes complex conjugation; e.g., $\bar{z} = x - iy$ is the complex conjugate of z).

The function $f(z)$ corresponds to the following velocity profile:

$$u(z, \bar{z}) \equiv v_y + iv_x = \frac{eNV}{8\eta i} \left[\frac{z\bar{z} - C}{\sqrt{z^2 - w^2}} + \sqrt{\bar{z}^2 - w^2} \right], \quad (11)$$

with an undetermined constant C .

One surprising feature of Eq. (11), derived in the no-stress limit, is that the velocity profile is not uniquely determined. A closer inspection [see Appendix A for the analysis leading to Eq. (11)] shows that this family exhausts all solutions with vorticity and electric potential integrable in the vicinity of the slit endpoints. However, there exist other solutions to this problem, which have non-integrable vorticity, but finite total current passing through the slit, see Eq. (35), and infinitely many even more singular solutions, which support infinite current at a finite voltage drop (see Appendix B).

In Ref. [48] the coefficient C was fixed by comparing the velocity distribution given by Eq. (11) at $r \rightarrow \infty$ to that previously obtained for a point contact, $w \equiv 0$ [44], leading to

$$C = 2w^2. \quad (12)$$

We will argue in what follows that this choice is problematic, as it leads to the solution that is internally inconsistent (in particular, not respecting the energy conservation law). Moreover, we will show that the point-contact limit itself is not well-defined.

III. WORK, DISSIPATION, AND ENERGY CONSERVATION

In this section, we take a closer look at the solution in Eq. (11) obtained under the requirement of vanishing stress-tensor at the boundaries of the barrier and integrable vorticity. It is useful to express the dissipation power stemming from viscosity as a function of complex variables. Using Eq. (5), we get

$$P(z, \bar{z}) = 4\eta \frac{\partial u}{\partial z} \cdot \frac{\partial \bar{u}}{\partial \bar{z}}. \quad (13)$$

Another useful representation [52, 53] for viscous dissipation is through vorticity, Eq. (7):

$$P(x, y) = \eta \omega^2 + 2\eta \nabla \cdot (\mathbf{v} \cdot \nabla) \mathbf{v}. \quad (14)$$

Integrating by parts, one may show that under suitable conditions (fulfilled in our case), the total dissipated power reads as

$$\mathcal{P} \equiv \iint P(x, y) dx dy = \eta \iint \omega^2(x, y) dx dy. \quad (15)$$

In the vicinity of the slit endpoints, Eqs. (11) and (13) give for the leading term of the dissipation power:

$$P(z, \bar{z}) \propto \frac{(w^2 - C)^2}{w} \left| \frac{\partial(z \pm w)^{-\frac{1}{2}}}{\partial z} \right|^2 \propto \frac{(w^2 - C)^2}{R^3}, \quad (16)$$

where $R = \sqrt{(x \pm w)^2 + y^2}$ denotes the distance from the slit endpoints. For general choices of C , Eq. (16) diverges $\sim 1/R$ after the integration over z and \bar{z} , when R approaches zero. This divergence disappears if and only if $C = w^2$. This choice is different from that based on the matching of the velocity profile at large distances to the point-contact asymptotics, Eq. (12), as was done starting with the no-stress requirement at the barrier in Ref. [48]. Note that the velocity profile with $C = w^2$ under the no-stress requirement is equivalent to the so called ‘‘no-slip’’ solution derived in Ref. [5], which assumed zero velocity at the barrier. It turns out that this no-slip solution is simultaneously characterized by zero stress at the boundary, and, thus, is a valid no-stress solution, too.

The divergence of dissipation for $C \neq w^2$ is accompanied by a divergence of velocity near two slit endpoints, as shown in Fig. 2. To see this explicitly, we evaluate the velocity near the right end of the slit using polar coordinates ρ and φ defined as

$$y = \rho \sin \varphi, \quad x = w - \rho \cos \varphi. \quad (17)$$

Here, $\varphi = 0$ in the slit (i.e., for $y = 0$ and $x < w$), and grows clockwise. When close enough to the slit right end ($\rho \ll w$), the velocity reads

$$\begin{aligned} v_x &= \frac{eNV}{4\eta} \sqrt{2\rho w} \left(\cos^2 \frac{\varphi}{2} \sin \frac{\varphi}{2} - \frac{w^2 - \mathcal{C}}{4w\rho} \sin \frac{\varphi}{2} \right) \\ v_y &= \frac{eNV}{4\eta} \sqrt{2\rho w} \left(\cos^3 \frac{\varphi}{2} - \frac{w^2 - \mathcal{C}}{4w\rho} \cos \frac{\varphi}{2} \right). \end{aligned} \quad (18)$$

Equation (18) is valid once $|\varphi| < 2 \arccos [(\rho/4w)^{1/4}]$, otherwise the next-leading order contribution is not negligible. Clearly, when $\mathcal{C} \neq w^2$, velocities diverge as $v_x, v_y \sim \rho^{-1/2}$ near the slit endpoints.

In agreement with Ref. [48], the value of \mathcal{C} also changes the velocity profiles away from the slit. Indeed, with a general value of \mathcal{C} , velocities at large distances $|z| \gg w$ become

$$\begin{aligned} v_x &\approx v_r \left(\frac{xy^2}{r^3} - \frac{w^2 - \mathcal{C}}{2w^2} \frac{x}{r} \right), \\ v_y &\approx v_r \left(\frac{y^3}{r^3} - \frac{w^2 - \mathcal{C}}{2w^2} \frac{y}{r} \right), \end{aligned} \quad (19)$$

where $v_r = eNVw^2/(4r\eta)$.

Noticeably, when $\mathcal{C} = w^2$, following Eq. (11), $v_x(x, 0) = \partial_y v_x(x, y)|_{y=0} = 0$ at the boundary, indicating that both the no-slip and no-stress boundary conditions are satisfied simultaneously. As seen from asymptotic Eq. (19), this happens because v_x tends to zero very quickly, $\propto y^2$, when approaching to the boundary. Importantly, the slip length entering partial-slip boundary condition, Eq. (3), turns out to be irrelevant and does not enter into solution for velocity. Indeed, when both the velocity and the shear stress are equal identically to zero, the equality of Eq. (3) holds for an arbitrary value of λ . It is also worth stressing that large-distance behavior given by Eq. (19) for $\mathcal{C} = w^2$ does not coincide with behavior obtained in Ref. [44] within the ‘‘point-source’’ model, see discussion in Appendix C.

Let us discuss the energy balance for the case of $\mathcal{C} = w^2$. The dissipation power [in polar coordinates (r, θ) centered at $x = y = 0$ with $\theta = 0$ corresponding to $x > 0, y = 0^+$] reads

$$P(r, \theta) = \frac{(eNVw^2)^2}{16\eta} \frac{4r^2 \sin^2(\theta)}{[r^4 + w^4 - 2w^2r^2 \cos(2\theta)]^{3/2}}. \quad (20)$$

Near the slit endpoints it becomes

$$P \propto 1/\sqrt{(x \pm w)^2 + y^2} \sim 1/R \quad (21)$$

and is thus integrable. The total dissipated power for the solution with $\mathcal{C} = w^2$ reads

$$\mathcal{P} = \frac{\pi}{8} \frac{(eNVw)^2}{\eta}. \quad (22)$$

From energy conservation, the dissipated power equals to the energy supply V^2/R (Joule law). We thus obtain

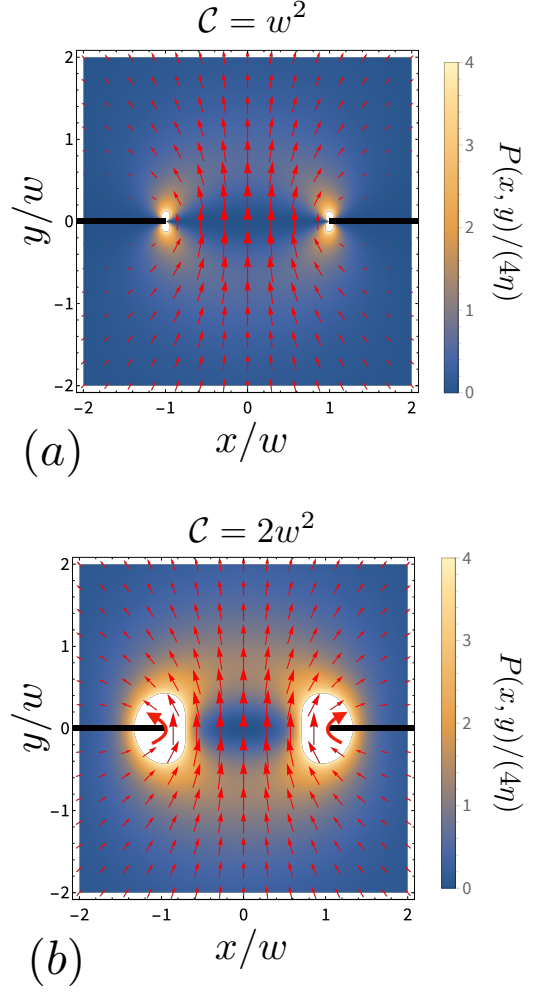


FIG. 2. Velocity and dissipation profiles for (a) $\mathcal{C} = w^2$, and (b) $\mathcal{C} = 2w^2$. The velocity directions and the magnitudes are shown by the direction and scale of red arrows, respectively. Note that the velocity streamlines are the same in both panels; the difference is only in the velocity magnitudes. In panel (b), with the choice $\mathcal{C} = 2w^2$ (as in Ref. [48]), the velocity diverges near the slit ends (as indicated by the thickest arrows), leading to a stronger divergence in the dissipation power ($1/R^3$ for $\mathcal{C} = 2w^2$ vs. $1/R$ for $\mathcal{C} = w^2$, where R is the distance to the endpoint of the slit), cf. Eqs. (16) and (21). As a result, the space-integrated dissipation power, while being finite for $\mathcal{C} = w^2$, diverges for $\mathcal{C} = 2w^2$. In fact, a similar dissipation profile, leading to the divergence of the total dissipation, is established for any $\mathcal{C} \neq w^2$.

the resistance from viscosity-induced dissipation

$$R = \frac{8}{\pi} \frac{\eta}{e^2 N^2 w^2}, \quad (23)$$

We can compare this result with the direct calculation of resistance. Inside the slit, the solution (11) with $\mathcal{C} = w^2$ yields

$$v_y(x, y = 0) = \frac{eNV}{4\eta} \sqrt{w^2 - x^2}, \quad |x| < w.$$

Then, for the total current, we have

$$I = eN \int_{-w}^w v_y(x, 0) dx = \frac{(eNw)^2 V \pi}{8\eta}. \quad (24)$$

By the direct definition of the resistance, we find

$$R = \frac{V}{I} = \frac{8\eta}{\pi e^2 N^2 w^2} = R_{\text{no-slip}},$$

where $R_{\text{no-slip}}$ was obtained in Ref. [5] for no-slip boundary condition. This result coincides with the result obtained from the dissipation, Eq. (23), indicating consistency of our analysis.

Let us discuss this point in more detail. There exist at least three different methods to obtain the viscosity-induced resistance: (i) via evaluating the total viscosity-induced dissipation power $R_P = V^2/\mathcal{P}$; (ii) via the definition of the resistance, i.e., $R = V/I$, where I is the total current through the slit; and (iii) via evaluating the total work W done by the electric force: $R_W = V^2/W$. Above we have proved the agreement between resistance obtained from methods (i) and (ii). We will now show that the total work done by the electric force equals to the dissipation caused by viscosity.

The local work done by the electric field (\mathbf{E}) can be found from the Stokes equation:

$$\begin{aligned} Ne\mathbf{v} \cdot \mathbf{E} &= -Ne\mathbf{v} \cdot \nabla\phi = -\eta\mathbf{v} \cdot \nabla^2\mathbf{v} \\ &= -\eta [v_x (\partial_x^2 + \partial_y^2) v_x + v_y (\partial_x^2 + \partial_y^2) v_y] \\ &= -2\eta \left[u \frac{\partial^2}{\partial z \partial \bar{z}} \bar{u} + \bar{u} \frac{\partial^2}{\partial z \partial \bar{z}} u \right]. \end{aligned} \quad (25)$$

The total work done by the electric force is equal to the integral of Eq. (25) over space, i.e.,

$$\begin{aligned} W &= Ne \iint dx dy \mathbf{v} \cdot \mathbf{E} \\ &= -4\eta \int d\bar{z} u \partial_{\bar{z}} \bar{u} \Big|_{\text{boundary}} - 4\eta \int dz \bar{u} \partial_z u \Big|_{\text{boundary}} \\ &\quad + 4\eta \iint dx dy \frac{\partial u}{\partial z} \frac{\partial \bar{u}}{\partial \bar{z}}, \end{aligned} \quad (26)$$

where the second line refers to boundary contributions. Following Eq. (19) for the velocity profile away from the slit, the work of electric field at infinity is negligible. Further, we can see from our solution (11) with $\mathcal{C} = w^2$ that the contribution to the total work from the boundary of the barrier also equals to zero. The last term in Eq. (26) exactly equals to the total dissipation power produced by viscosity, Eqs. (13) and (22), $W = \mathcal{P}$, hence, $R_W = R_P$. We have thus proven that the resistance evaluated by all the three methods is the same.

In contrast, these three quantities are different for the velocity profile obtained in Refs. [44, 48] for the no-stress boundary condition with Eq. (12). To start with, Eq. (16) indicates that at $\mathcal{C} = 2w^2$, the dissipation power near the end of the slit has a singularity that

generates a divergent total dissipation. The viscous resistance R obtained from method (i) introduced above (i.e., $R_P = V^2/\mathcal{P}$) vanishes, because of the divergence of total dissipation \mathcal{P} . Interestingly, if one fixes the total current I rather than the voltage V , if resistance is defined as \mathcal{P}/I^2 , it would diverge for $\mathcal{C} = 2w^2$. This discrepancy indicates that the choice $\mathcal{C} = 2w^2$ (as well as any other choice $\mathcal{C} \neq w^2$) is physically unreasonable unphysical, although it satisfies the Stokes equation with the no-stress boundary conditions, and gives finite current through the slit. At the same time, resistances $R = V/I$ and R_W obtained for $\mathcal{C} = 2w^2$ from methods (ii) and (iii), respectively, are both finite, but are not equal to each other. Indeed, Ref. [48] reports a finite viscous resistance $R_{\text{no-stress}} = R_{\text{no-slip}}/2$ following method (ii), i.e., with the resistance defined as V/I . The resistance R_W , however, is equal to $2R_{\text{no-slip}}/3$, when it is obtained by method (iii) from the total work of the electric field ($R = V^2/W$) in the bulk of the sample (see Appendix D).

Let us note that the contribution to velocity of terms proportional to $(\mathcal{C} - w^2)$ [e.g., the second terms of Eqs. (18), (19)] does not produce any electric field in the sample, as follows from Eq. (4). Indeed, the whole family of solutions Eq. (11) is characterized by the same electric potential. Thus, the situation with the velocity terms $\propto (\mathcal{C} - w^2)$ is similar to the one encountered in Ref. [6], where the velocity profile is characterized by the coexistence of zero electric field and finite viscous dissipation in the bulk of the sample. In that paper, the energy conservation was fixed by the presence of a potential jump (infinite electric field) at the interface between the sample and metallic contact. It is clear, however, that in a realistic setup with metallic contacts in the slit geometry, the divergent (for $\mathcal{C} \neq w^2$) total viscous dissipation power cannot be balanced by any finite potential jump at the interfaces with metallic contacts.

IV. ANALYSIS OF THE PROBLEM AT ARBITRARY SLIP LENGTH

Interestingly, although the solution in Eq. (11) is obtained under the no-stress boundary condition, for $\mathcal{C} = w^2$ it also solves the general flow problem at arbitrary λ , including the no-slip limit as a particular case. However, there is a question about the uniqueness of this solution in the general case of arbitrary slip length λ , which cannot be answered without a general solution.

Assuming that the total current through the slit is finite and the velocity is integrable at the $y = 0$ boundary, we can express the velocity profile $\vec{v}(x, y) = (v_x(x, y), v_y(x, y))$ through $v_x(x, 0)$ and $v_y(x, 0)$:

$$\begin{aligned} \vec{v}(x, y) &= \int \vec{K}_1(x - x', y) v_x(x', 0) dx' \\ &\quad + \int \vec{K}_2(x - x', y) v_y(x', 0) dx' \end{aligned} \quad (27)$$

with kernels

$$\begin{aligned}\vec{K}_1(x-x', y) &= \frac{2(x-x')y}{\pi[(x-x')^2 + y^2]^2} \begin{pmatrix} x-x' \\ y \end{pmatrix}, \\ \vec{K}_2(x-x', y) &= \frac{2y^2}{\pi[(x-x')^2 + y^2]^2} \begin{pmatrix} x-x' \\ y \end{pmatrix}.\end{aligned}\quad (28)$$

Derivation of these kernels is presented in Appendix E.

The boundary velocities should be found by imposing the boundary conditions. The first condition is given by Eq. (3) and the second condition comes from the requirement of symmetry along $y = 0$ axis:

$$\partial_y^2 v_x(x, y)|_{y=0, |x|<w} = 0.$$

It is convenient that the boundary velocities are defined on disjoint sets: (i) as the wall is impenetrable, we have $v_y(x, 0) \equiv 0$ for $|x| > w$, (ii) from the symmetry of the problem, we have $v_x(x, 0) \equiv 0$ for $|x| < w$. After imposing these boundary conditions, we get the following integral equations:

$$\begin{aligned}v_x(x, 0) &= \frac{4\lambda}{\pi} \frac{\partial}{\partial x} \int_w^\infty \frac{x'}{x'^2 - x^2} v_x(x', 0) dx', \\ 0 &= \frac{\partial^2}{\partial x^2} \int_{-w}^w \frac{1}{x' - x} v_y(x', 0) dx'.\end{aligned}\quad (29)$$

Integrating both parts of the first equation over x , we get

$$\int_w^\infty v_x(x', 0) dx' = -\frac{4\lambda}{\pi} \int_w^\infty \frac{x'}{x'^2 - w^2} v_x(x', 0) dx'.$$

If we are looking for the solution, for which $v_x(x, 0)$ does not change its sign on the wall (this is a reasonable assumption for a viscous flow without turbulence), the only possible solution is $v_x(x, 0) = 0$. Actually, this can be rigorously proved assuming integrable dissipation near the slit endpoints, see Appendix F. Thanks to the symmetry $v_y(x, y) = v_y(-x, y)$ the second equation is equivalent to

$$\int_{-w}^w \frac{1}{x' - x} v_y(x', 0) dx' = -\pi c_1 x. \quad (31)$$

This is a singular integral equation, for which the general solution is known and can be found, e.g., in Ref. [54]. This solution allows for the square-root and inverse square-root dependencies on $1 - x^2/w^2$:

$$v_x(x, 0) = 0, \quad v_y(x, 0) = c_1 \sqrt{w^2 - x^2} + \frac{c_2}{\sqrt{w^2 - x^2}}. \quad (32)$$

The no-stress $\lambda \rightarrow \infty$ limit is singular. In this limit, the first line of Eq. (29) reduces to

$$\frac{\partial}{\partial x} \int_w^\infty \frac{x'}{x'^2 - x^2} v_x(x', 0) dx' = 0. \quad (33)$$

This equation actually allows nonzero solutions with velocity which does not change sign on the wall. From

Eq. (F1), we find, that the corresponding family of solutions for $v_x(x, 0)$ is [54]

$$v_x(x, 0) = c_3 \frac{\text{sign}(x)}{\sqrt{x^2 - w^2}} \quad (34)$$

and $v_y(x, 0)$ the same as in Eq. (32). Notice, that this family of solutions is larger than obtained for the no-stress case in Sec. II, Eq. (11). Indeed, computing the velocity in the whole plane, we find for the general no-stress solution:

$$u(z, \bar{z}) \equiv v_y + i v_x = \sum_{k=1}^3 c_k U_k(z, \bar{z}), \quad (35)$$

where

$$U_1(z, \bar{z}) = \frac{1}{2i} \left(\sqrt{\bar{z}^2 - w^2} + \frac{z\bar{z} - w^2}{\sqrt{z^2 - w^2}} \right), \quad (36)$$

$$U_2(z, \bar{z}) = \frac{i}{2} \left(\frac{2z^2 - z\bar{z} - w^2}{(z^2 - w^2)^{3/2}} + \frac{1}{\sqrt{\bar{z}^2 - w^2}} \right) \quad (37)$$

and

$$U_3(z, \bar{z}) = -\frac{i}{2} \left(\frac{w^2 - z\bar{z}}{(z^2 - w^2)^{3/2}} + \frac{1}{\sqrt{\bar{z}^2 - w^2}} \right). \quad (38)$$

We thus see that the solution delivered by Eq. (11) is reproduced at:

$$c_1 = \frac{eNV}{4\eta} \quad \text{and} \quad c_2 = c_3 = \frac{eNV}{8\eta} (C - w^2). \quad (39)$$

We notice that the voltage drop across the sample, $V = V(y = \infty) - V(y = -\infty)$, corresponding to the solution Eq. (35) depends on the coefficient c_1 only: $V = (4\eta/eN)c_1$. Finally, computing vorticity,

$$\omega(z, \bar{z}) = 2\text{Im} \left[c_1 \frac{z}{\sqrt{z^2 - w^2}} + (c_2 - c_3) \frac{z}{(z^2 - w^2)^{3/2}} \right], \quad (40)$$

we find that the solutions with $c_2 \neq c_3$ have non-integrable divergence of vorticity, and, therefore, do not follow the Keldysh-Sedov theorem.

Inspecting the velocity profiles of Eq. (35), we find that the solution with finite dissipation is unique and is identical to the one delivered by Eq. (11) at $C = w^2$. This solution in fact satisfies both the no-slip and no-stress boundary conditions. As discussed in Appendix C, this solution cannot be captured by using the partial-slip ‘‘point-source’’ solution with $w \equiv 0$ (Ref. [44]).

V. TEMPERATURE PROFILES

With the velocity profiles of Eq. (11), in this section, we derive the corresponding temperature distribution. We start with noting that the electronic heat transfer

in the hydrodynamic regime strongly depends on the spectrum. In particular, for relativistic dispersion, the electron-electron scattering does not affect the energy current, as it is represented through the total momentum conserved by scatterings [3]. On the contrary, for the parabolic dispersion, electron-electron scattering is capable of establishing a finite thermal conductivity without extra momentum-relaxing scattering events. Here, we limit ourselves with discussion of the parabolic spectrum only. Heat transfer in the system of Dirac fermions will be discussed elsewhere.

For parabolic dispersion, the temperature obeys the heat-balance equation [55]

$$-\kappa\nabla^2\delta T + C(\mathbf{v}\cdot\nabla)\delta T = P(x, y) - N\gamma\delta T. \quad (41)$$

Here, $\delta T \equiv T - T_0$ refers to the temperature variation with respect to the background temperature T_0 , κ is the heat conductivity, C the heat capacity, and γ denotes the electron-phonon coupling constant. The ‘‘convection’’ term, $\text{div}(\mathbf{v}T) = (\mathbf{v}\cdot\nabla)\delta T$, which breaks the particle-hole symmetry, is known to introduce an asymmetry in the temperature distribution [56, 57]. Throughout this section, we consider the regular (no-stress-no-slip) velocity profile, i.e., Eq. (11) with $C = w^2$, which is the unique choice that produces a finite total dissipation, as discussed above.

Generally, it is difficult to obtain the full solution of Eq. (41). Here, for simplicity, we focus on the two limiting cases of small and large heat conductivity.

A. Small heat conductivity

In this section, we ignore the heat conductivity (i.e., we take $\kappa = 0$). Then, equation (41) reduces to

$$C\left(v_x\frac{\partial\delta T}{\partial x} + v_y\frac{\partial\delta T}{\partial y}\right) = P(x, y) - N\gamma\delta T \quad (42)$$

Using the method of characteristics and switching to the complex coordinates, we find:

$$\begin{cases} C\frac{d\delta T}{dt} = P(z, \bar{z}) - N\gamma\delta T, \\ \frac{dz}{dt} = i\bar{u}, \quad \frac{d\bar{z}}{dt} = -iu. \end{cases} \quad (43)$$

Here, the source term $P(z, \bar{z})$ is defined by Eq. (13) and t counts the ‘‘time’’ passed since the movement along the characteristic curve started.

Solutions of characteristic differential equations consist of a set of hyperbolas parametrized by r_0

$$\frac{x^2}{r_0^2} - \frac{y^2}{w^2 - r_0^2} = 1, \quad (44)$$

or, equivalently,

$$z\bar{z} + \sqrt{z^2 - w^2}\sqrt{\bar{z}^2 - w^2} = 2r_0^2 - w^2. \quad (45)$$

Geometrically, r_0 refers to the minimum distance from point $(0, 0)$ to a given characteristic curve. The following equation establishes the parameter r_0 of the characteristics passing through a given point (r, θ) :

$$r_0^2 = \frac{1}{2}\left(w^2 + r^2 - \sqrt{r^4 + w^4 - 2r^2w^2\cos 2\theta}\right). \quad (46)$$

The bounded solution along the characteristic satisfying $\delta T(-\infty) = 0$ can be found as follows:

$$\delta T(t) = \int_{-\infty}^t \frac{P(s)}{C} \exp\left[-\frac{N\gamma(t-s)}{C}\right] ds. \quad (47)$$

Using Eq. (45), we can rewrite the velocity and dissipation profiles as follows:

$$u(z, \bar{z}) = \frac{eNV}{4\eta i} \frac{r_0^2 - w^2}{\sqrt{z^2 - w^2}}, \quad (48)$$

$$P(z, \bar{z}) = \frac{(eNVw)^2}{4\eta} \frac{(w^2 - r_0^2)(z\bar{z} - r_0^2)}{(z\bar{z} + w^2 - 2r_0^2)^3}. \quad (49)$$

The dissipation pattern described by Eq. (49) is shown in Fig. 2(a). It is very convenient that along a given characteristic ($r_0 = \text{const}$) dissipation depends only on $r^2 = z\bar{z}$. Using Eqs. (43) and (48), we get the following differential equation for $r^2(t)$:

$$\frac{dr^2}{dt} = \pm \frac{eNV(w^2 - r_0^2)}{4\eta} \frac{\sqrt{(2r^2 + w^2 - 2r_0^2)^2 - w^4}}{r^2 + w^2 - 2r_0^2}, \quad (50)$$

with $+$ for the upper and $-$ for the lower half-planes, correspondingly. Solving this equation, we obtain the relation between the ‘‘time’’ on a characteristic curve and coordinates on the plane r, r_0 :

$$f(r^2) = \frac{eNV}{\eta} |t - t_0|, \quad (51)$$

where t_0 corresponds to the ‘‘time’’ in the slit ($y = 0$) and $f(r^2)$ is given by

$$\begin{aligned} f(r^2) = & \frac{\sqrt{[2(r^2 - r_0^2) + w^2]^2 - w^4}}{(w^2 - r_0^2)} + \\ & + \frac{w^2 - 2r_0^2}{w^2 - r_0^2} \text{arccosh}\left(1 + 2\frac{r^2 - r_0^2}{w^2}\right). \end{aligned} \quad (52)$$

We can now switch the integration variable in the integral (47) from ds to $u = dr^2$ to compute the temperature:

$$\delta T = \delta T(\mathbf{r}) = \begin{cases} \delta T_+(\mathbf{r}), & \text{for } y > 0, \\ \delta T_-(\mathbf{r}), & \text{for } y < 0, \end{cases} \quad (53)$$

where

$$\delta T_{\pm}(r_0, r) = \frac{\delta T_0(r_0) \pm \int_{r_0^2}^{r^2} I_{r_0}(u) e^{\pm\zeta f(u)} \frac{du}{w^2}}{e^{\pm\zeta f(r^2)}} \quad (54)$$

is expressed in terms of the temperature in the slit (i.e., at $y = 0$, $-w < x < w$):

$$\delta T_0(r_0) = \int_{r_0^2}^{\infty} I_{r_0}(u) e^{\zeta f(u)} \frac{du}{w^2} \quad (55)$$

where

$$I_{r_0}(u) = T_V \frac{w^4(u - r_0^2)}{(u + w^2 - 2r_0^2)^2 \sqrt{[2(u - r_0^2) + w^2]^2 - w^4}}, \quad (56)$$

and

$$\zeta = \frac{w^2}{l_{\text{vis}}^2}, \quad l_{\text{vis}} = \sqrt{\frac{eVC}{\eta\gamma}} w, \quad T_V = \frac{eNV}{C} \quad (57)$$

The last two expressions here define the spatial length scale l_{vis} of the heated area and the corresponding temperature scale T_V governing the variation of temperature in the heated region. The temperature profile given by Eq. (54) is illustrated in Fig. 3.

Far away from the slit, at $r \gg w$, we find

$$\delta T_{\pm}(r, \theta) = T_V \frac{w^2}{2r^2} g_{\pm} \left(\frac{2r^2}{l_{\text{vis}}^2 \sin^2 \theta} \right), \quad (58)$$

where $g_{\pm}(t) = t \exp(\mp t) \text{Ei}(\pm t) \mp 1$ and Ei is the exponential integral function. In the limit of $r \gg l_{\text{vis}} \sin \theta$, to the leading order of l_{vis}/r , the temperature distribution becomes symmetric between the half-planes:

$$\delta T_{\pm}(r, \theta) \approx T_V \frac{w^2 l_{\text{vis}}^2}{4r^4} \sin^2 \theta. \quad (59)$$

In this limit, the heat produced by the viscous dissipation is balanced by the phonon-emission, i.e., $\delta T \approx CP(x, y)/N\gamma$. In this case, the temperature δT and the velocity squared v^2 share the same features. Indeed, both of them decay as $\sim 1/r^4$ in space, with the directional distribution $\sim \sin^2 \theta$.

Let us now discuss the temperature distribution $\delta T_0(r_0 = r)$ in the slit (for $|x| < w$, $y = 0$), which can be found from Eq. (55) as

$$\delta T_0(r) = T_V F(\mathbf{x} = r/w)$$

with

$$F(\mathbf{x}) = \int_0^{\infty} \frac{udu}{2\sqrt{u(u+1)}(u+1-x^2)^2} \times \exp \left\{ \frac{-\zeta \left[(1-2x^2) \text{arccosh}(2u+1) + 2\sqrt{u(u+1)} \right]}{1-x^2} \right\} \quad (60)$$

a function of the dimensionless variable $\mathbf{x} \equiv x/w$. We plot $F(\mathbf{x})$ in Fig. 4, for different ζ values.

In the limit $\zeta \sqrt{1-x^2} \gg 1$, the integral in Eq. (60) is dominated by $u \ll 1$ resulting into

$$F(\mathbf{x}) \approx \frac{1}{32\zeta^3(1-x^2)^2}. \quad (61)$$

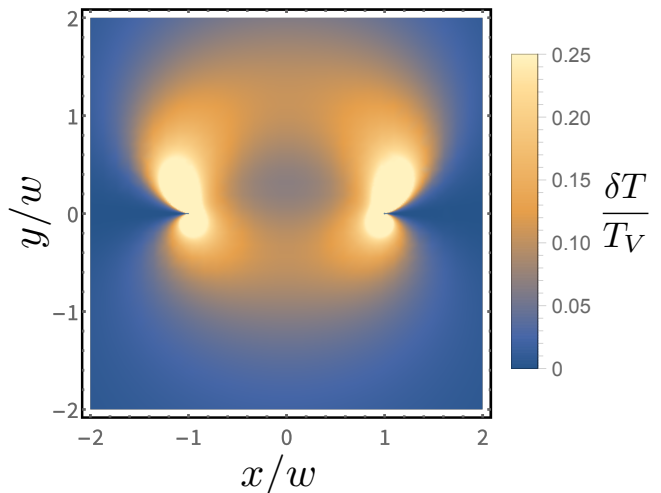


FIG. 3. Heatmap of the nonequilibrium variation of the temperature δT [defined in Eq. (53)], computed according to Eq. (54) for the velocity profile with $C = w^2$ and $l_{\text{vis}} = 2w$. The temperature is measured in units of T_V , see Eq. (57). Because of the divergence of δT near the slit endpoints, the values are clipped at $\delta T = T_V/4$ for better visibility. The temperature profile, compared to the dissipation power shown in Fig. 2(a), shows the $y \rightarrow -y$ asymmetry induced by the nonlinear character of the convection term in the heat-balance equation [47, 56, 57].

In the opposite limit, $\zeta \sqrt{1-x^2} \ll 1$, the exponential factors in Eq. (54) can be neglected. This gives for $F(\mathbf{x})$ the following approximation:

$$F(\mathbf{x}) \approx \frac{1}{2x^3} \left[\frac{\arcsin(\mathbf{x})}{\sqrt{1-x^2}} - \mathbf{x} \right]. \quad (62)$$

This function has the following limiting behaviors:

$$F(0) = 1/3, \quad F(\mathbf{x} \rightarrow 1) \approx \frac{\pi}{4\sqrt{2}} (1-x)^{-1/2}, \quad (63)$$

indicating a weak divergence of temperature upon approaching the slit edge.

Let us consider the temperature distribution near the slit but away from the $y = 0$ line, in the coordinates of Eq. (17). In this case, the characteristics can be expressed as

$$\rho = \rho_0 \frac{1}{\cos^2 \frac{\varphi}{2}}, \quad (64)$$

where ρ and φ refer to the polar-coordinate variables defined in Eq. (18). Each characteristic curve is labelled by its smallest distance ρ_0 to the right end of the slit. We can now study the temperature distribution along each characteristics, as a function of φ . Indeed, following the introduced general method, the temperature near the

endpoint of the slit is given approximately by

$$\begin{aligned} \mathcal{T}(\varphi) = \mathcal{T}(\varphi_0) \exp \left\{ -\frac{4w^2}{l_{\text{vis}}^2} \chi [\xi(\varphi) - \xi(\varphi_0)] \right\} \\ + \frac{1}{4\chi} \int_{\varphi_0}^{\varphi} d\varphi' \sin^2 \frac{\varphi'}{2} \exp \left\{ \frac{4w^2}{l_{\text{vis}}^2} \chi [\xi(\varphi') - \xi(\varphi)] \right\}, \end{aligned} \quad (65)$$

where $\mathcal{T} \equiv \delta T/T_V$ is the dimensionless temperature,

$$\chi \equiv \frac{N}{C} \sqrt{\frac{\rho_0}{2w}}, \quad (66)$$

φ_0 is the starting point of the integral, and

$$\xi(\varphi) = 2 \tan \frac{\varphi}{2} \left(1 + \frac{1}{3} \tan^2 \frac{\varphi}{2} \right) \quad (67)$$

is the angular distribution function.

When $\varphi_0 < \varphi$, the integral is along the transport direction of particles; otherwise, the integral is against the particle traveling direction. It is convenient to choose $\varphi_0 = 0$, since we know the temperature distribution inside the slit and near the edges ($\rho_0 \ll w/\zeta^2$) from Eq. (62). Therefore,

$$\mathcal{T}(\varphi_0) = \mathcal{T}(0) = T_V \frac{\pi}{8} \sqrt{\frac{2w}{\rho_0}}. \quad (68)$$

The most interesting result here is the temperature divergence in the vicinity of the slit endpoints: $T \propto \rho^{-1/2}$. The divergence is cured by taking into account finite heat conductivity. For very small but finite heat conductivity, diffusion term in the heat balance equation can be neglected everywhere except narrow regions near the endpoint of the slit. Indeed, after neglecting the angle dependence, this term is estimated as $\kappa \rho^{-2} \delta T$ near the slit endpoint. In comparison, since the velocity $\mathbf{v} \sim \sqrt{\rho}$ [see Eq. (18)], the convection term is proportional to $\rho^{-1/2}$ and grows much slower than the heat diffusion contribution upon approaching the endpoint. Consequently, the diffusion contribution dominates at positions close enough to the slit ends even for very small κ . By comparing two terms on the left side of Eq. (41), one finds that the diffusion comes into play for

$$\rho < w \left(\frac{\kappa \eta}{e N C V w^2} \right)^{\frac{3}{2}}.$$

Figures 5(a), (b), and (c) show the temperature profiles of the same characteristic curve $\chi = 0.01$. When l_{vis} decreases (corresponding to a smaller driving), a two-peak structure of the temperature profile begins to emerge, and becomes apparent in Fig. 5(c). In Fig. 5(d), we take the same ratio l_{vis}/w as that in Fig. 5(b), but use a smaller value of $\chi = 0.005$. The corresponding shapes of the temperature profile of Figs. 5(b) and (d) are rather similar. However, the temperature values in Fig. 5(d) almost double, in agreement with the $\sim 1/\sqrt{\rho_0}$ dependence near the endpoint of the slit [see Eq. (68)].

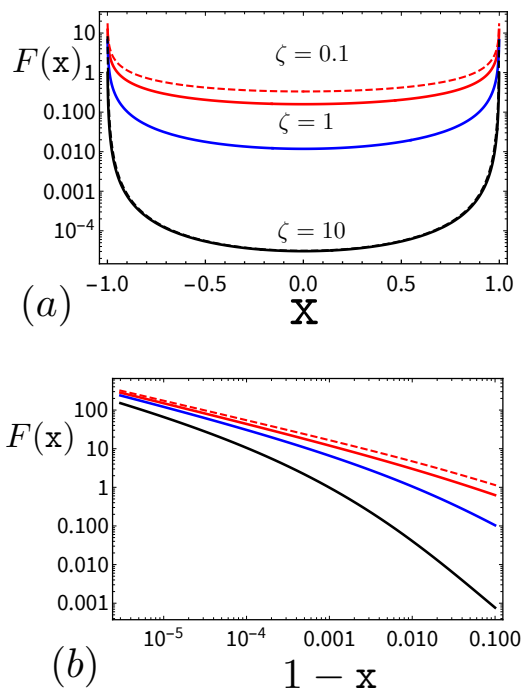


FIG. 4. (a) Curves of the function $F(\mathbf{x})$ [Eq. (60)] in the slit (solid lines), for $\zeta = 10$ (black), $\zeta = 1$ (blue) and $\zeta = 0.1$ (red). The red and black dashed lines show asymptotic results described by Eqs. (62) and (61), respectively. The red lines agree better near the slit ends; The black ones instead have a better overlap in the middle of the slit (the curves are almost indistinguishable). (b) The asymptotic feature of corresponding curves in panel (a) near the right end of the slit (i.e., $\mathbf{x} \rightarrow 1$). Near the slit endpoint, $F(\mathbf{x})$ curves with different ζ values approach the same (red dashed) line described by Eq. (62).

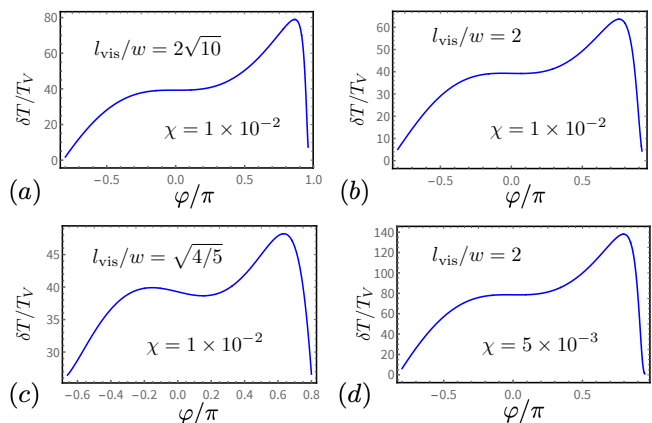


FIG. 5. Temperature distribution (in units of T_V) near the right end of the slit, with different choices of l_{vis}/w (different driving amplitude) and χ [different characteristics, see Eq. (66)]. (a) $l_{\text{vis}}/w = 2\sqrt{10}$ and $\chi = 0.01$; (b) $l_{\text{vis}}/w = 2$ and $\chi = 0.01$; (c) $l_{\text{vis}}/w = \sqrt{4/5}$ and $\chi = 0.01$, and (d) $l_{\text{vis}}/w = 2$ and $\chi = 0.005$.

B. Large heat conductivity

Now, we move on to the opposite limit of a large heat conductivity. In this limit, neglecting the convection term, the heat-balance equation takes the form

$$-\kappa \nabla^2 \delta T = P(x, y) - N\gamma \delta T. \quad (69)$$

Equation (69) can be solved by going into the momentum space, with the solution

$$\delta T(x, y) = \frac{1}{2\pi\gamma} \iint dx' dy' \mathcal{K}(x-x', y-y') P(x', y'), \quad (70)$$

where

$$\begin{aligned} \mathcal{K}(r) &= \int_0^\infty k dk \frac{1}{1 + \frac{\kappa}{n\gamma} k^2} J_0(kr) \\ &= \frac{1}{l_{\text{diff}}^2} K_0\left(\frac{r}{l_{\text{diff}}}\right). \end{aligned} \quad (71)$$

is the circularly symmetric kernel. In Eq. (71), J_0 and K_0 are the modified Bessel functions, of the first and second kinds, respectively.

In Eq. (71), we have defined another scale

$$l_{\text{diff}} \equiv \sqrt{\kappa/(N\gamma)}$$

that reflects the length scale of heat diffusion. Indeed, the value of l_{diff} increases in samples with either a strong heat conductivity κ , or a weak phonon emission rate γ . When γ decreases, heat diffuses to larger distances before being dissipated via phonon emissions. In contrast to l_{vis} that reflects non-equilibrium driving, l_{diff} is a sample-specific quantity that is defined already at equilibrium.

Now we are in a position to evaluate the temperature profile with Eqs. (20), (70), and (71). The kernel $\mathcal{K}(r')$ decays exponentially $\propto \exp(-r'/l_{\text{diff}})$ when r' becomes larger than l_{diff} . Consequently, for positions far away from the slit, $r \gg l_{\text{diff}}$, the temperature profile in the large heat-conductivity limit approximately equals to Eq. (59) for $\kappa = 0$, where temperature is proportional to the local dissipation power. By contrast, for small distances, $r \ll l_{\text{diff}}$, the temperature profiles for the two limiting cases of large and small κ are drastically different.

In the limit of a large heat conductivity, we work out the temperature profile via numerical integration of Eq. (70). The results are presented in Fig. 6, where

$$T_{\text{scale}} = e^2 NV^2 / (32\pi\gamma\eta)$$

is another temperature scale. Here we only show the temperature distribution of the upper half-plane $y > 0$ (since we excluded the convection contribution, temperature distribution is symmetric with respect to the $y = 0$ line). As seen from this figure, heat conductivity cures temperature singularities as expected.

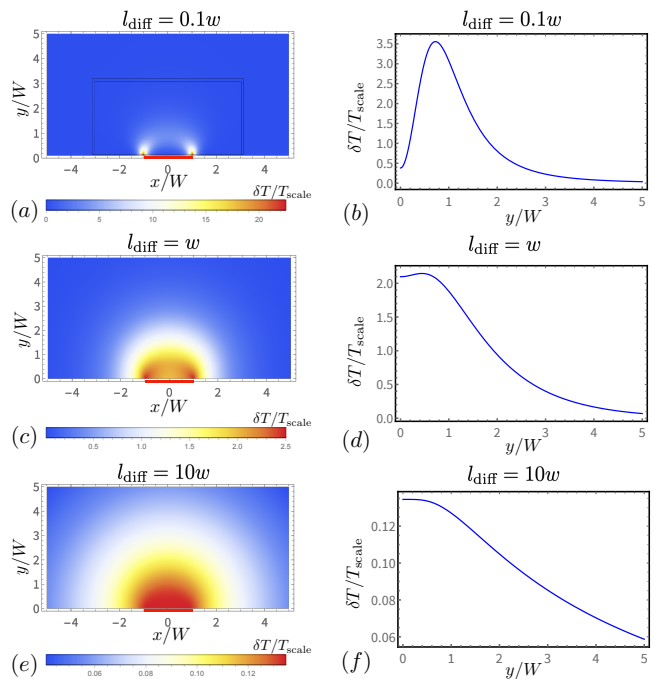


FIG. 6. Temperature distribution [in units of $T_{\text{scale}} = e^2 NV^2 / (32\pi\gamma\eta)$] of the upper half-plane of a sample with a strong diffusion. We provide only temperature profile of the upper half-plane, since the distribution is symmetric (with respect to $y = 0$) without contribution from the convection term. The slit has been marked out by the red solid line. We choose $l_{\text{diff}} = 0.1w$ for (a) and (b); $l_{\text{diff}} = w$ for (c) and (d); $l_{\text{diff}} = 10w$ for (e) and (f). Figures of the right panel present temperature distribution at $x = 0$, when y changes. The tail of an exponentially decaying temperature is clear in (b) and (d), but missing in (f).

The temperature profile is strongly influenced by the distance ratio l_{diff}/w . When $l_{\text{diff}} \ll w$, most dissipation-induced heating is transferred into phonons before diffusion in space, and the area with hot electrons is strongly confined near two endpoints of the slit, as shown in Figs. 6(a) and (b) for $l_{\text{diff}} = 0.1w$. Here, the temperature profile shows a clear ring-shape structure. When l_{diff} increases, the heated area begins to extend. When $l_{\text{diff}} = w$ [Figs. 6(c) and (d)], the heated area is slightly larger than the slit size w , although the strong heating near slit endpoints remains clearly visible. Finally, when $l_{\text{diff}} = 10w$, phonon emission is negligible at the scale of the slit width w , and the area with hot electrons becomes extensive. In Figs. 6(b), (d) and (f), we show the temperature distribution at $x = 0$ as a function of y : one sees that temperature decays slower in systems with a larger κ or l_{diff} .

VI. SUMMARY AND DISCUSSION

To summarize, we have investigated viscous hydrodynamic transport of electrons in a clean two-dimensional

sample between two semi-infinite planes separated by an impenetrable barrier with a finite-size slit. We have calculated the velocity profile assuming that a driving voltage is applied between these planes. We demonstrate that the standard boundary conditions at the barrier, say “no-stress”, together with the condition on the given voltage drop across the sample cannot uniquely determine the velocity. There exist infinitely many solutions satisfying these conditions. Among all possible solutions, we have found the unique one that leads to a finite total dissipated power, thus respecting the energy conservation. Our central result is that this only physical solution, which is characterized by a finite current through the slit and yields finite total dissipation, obeys *simultaneously* both the “no-slip” and “no-stress” boundary conditions. This in turn means that the slip length, which is often used for the partial-slip (Maxwell) boundary condition, is irrelevant for this problem and does not enter any physical result.

Several comments are in order here to compare this result with previous theoretical studies. The resistance of this “no-slip, no-stress” solution equals to the “superballistic” resistance obtained in Ref. [5] for the same system with the no-slip boundary condition. The distribution of the velocity in the slit calculated in Ref. [5] coincides with the corresponding distribution in our solution. However, the velocity profile in the whole plane was not reported in Ref. [5] (although, distribution far from the slit was found within the point-contact approximation in Ref. [44]). The fact that this solution also satisfies the no-stress condition (2) was not mentioned there. At the same time, in Ref. [48], a solution was found, which satisfies the no-stress condition (2), but does not satisfy the no-slip condition (1). As we demonstrated above, this solution yields a divergent total dissipation and, therefore, is nonphysical.

We have used the obtained velocity flow to solve the heat balance equation and investigate evolution of the electronic temperature profile while changing the heat conductivity. We have found that the overheated areas appear near the slit endpoints. The shape of these areas is determined by a competition between heat diffusion and heat convection. For a large heat conductivity, the diffusion dominates and these areas are approximately symmetric with respect to the barrier separating the two half-planes. In addition, by increasing the heat conductivity, we see a crossover between the ring-shape and the extended temperature profiles. Increasing the voltage (and, hence, the role of convection) leads to two effects: enhancement of asymmetry of the temperature pattern along the lines of the hydrodynamic flow and increase of the overheating. In the limit of zero heat conductivity, the temperature at the slit endpoints diverges. This divergence is cured by a finite heat conductivity. Our predictions can be directly verified experimentally with the use of recently developed ultra-precise techniques for simultaneous nanoimaging of temperature and current distributions [24, 34–42].

ACKNOWLEDGMENTS

We thank Igor Gornyi as one of the authors of the original idea, for an enormous contribution to this work and his unmeasurable kindness. We also thank Igor Burmistrov for the idea to use Keldysh-Sedov theorem in the analysis of this problem. The work of VK was supported by the Russian Science Foundation (Grant No. 20-12-00147).

Appendix A: Potential, vorticity, and velocity from Keldysh-Sedov’s formula

In this Appendix, we derive the family of solutions for the velocity profile that satisfies the no-stress boundary condition on the walls. Following Ref. [48], we take as the boundary conditions (i) Eq. (6) for electric potential at infinity; (ii) the symmetry requirement for the electric potential in the slit $\phi = V/2$, and (iii) the no-stress boundary condition, which results in the condition of zero vorticity on the walls

$$\omega = \left(\frac{\partial v_y}{\partial x} - \frac{\partial v_x}{\partial y} \right) \Big|_{|x|>w, y=0} = 0 \quad (\text{A1})$$

With these conditions, we get for the complex function in Eq. (9)

$$\begin{aligned} \text{Re}f(z)|_{|x|<w, y=0} &= -\frac{eV}{2\eta}, \\ \text{Im}f(z)|_{|x|>w, y=0} &= 0, \\ f(z)|_{r \rightarrow \infty} &= 0, \end{aligned} \quad (\text{A2})$$

and for the velocity field

$$\begin{aligned} v_y &= 0|_{|x|>w}, \\ v_x &= 0|_{|x|<w}. \end{aligned} \quad (\text{A3})$$

Thus, the problem is reduced to finding a holomorphic function in the complex half-plane with the known real part on the segment $y = 0$, $-w < x < w$ and imaginary part on the $y = 0$, $|x| > w$. The solution to this problem is given by the Keldysh-Sedov theorem [51]. This theorem states that there are no solutions that are finite near the points $(-w, 0)$ and $(w, 0)$. Furthermore, it allows one to express all possible solutions to the problem of finding $f(z)$ analytic in the upper half-plane under conditions of Eq. (A2) with finite $\int_{\tilde{z}} f(z) dz$ as follows:

$$f(z) = \frac{NeV}{2\eta} \left[-1 + \frac{z}{\sqrt{z^2 - w^2}} \right] + \frac{C_1}{\sqrt{z^2 - w^2}}. \quad (\text{A4})$$

We may now compute the velocity profile. Using the continuity equation $\nabla \cdot \mathbf{v} = 0$ for incompressible liquid and definition of vorticity, one arrives at the expression

$$\partial_{\tilde{z}}(v_y + iv_x) = \frac{1}{2} \text{Im}f(z). \quad (\text{A5})$$

Then, by definition,

$$u(z, \bar{z}) \equiv v_y + iv_x = \frac{1}{2} \int_{\bar{z}}^{\bar{z}} [\text{Im}f](z, \bar{z}) d\bar{z} + C(z), \quad (\text{A6})$$

where $C(z)$ is an arbitrary function, holomorphic in the upper half-plane. We can see that the part proportional to \mathcal{C}_1 leads to the logarithmic growth of velocity at infinity. Therefore we should put $\mathcal{C}_1 = 0$. Equation (A3) fixes the imaginary part of $C(z)$ on the segment $y = 0$, $-w < x < w$ and real part on the segment $y = 0$, $|x| > w$. This allows us to once again use Keldysh-Sedov's formula to compute $C(z)$ and arrive at Eq. (11) with \mathcal{C} an undetermined constant. Recall that in Eq. (11), we have chosen the branch cuts to run along the screen.

Let us note that real and imaginary parts of $f(z)$ deliver non-unique solutions to the Laplace equations $\Delta\phi = 0$ and $\Delta\omega = 0$, correspondingly. This non-uniqueness is related to the fact that the solutions diverge near the edges of the slit.

Appendix B: Singular solutions with nonintegrable total current obtained by an alternative method

In this Appendix, we briefly describe a method allowing to obtain general solutions obeying simultaneously both no-slip and no-stress boundary condition (more detailed discussion will be published elsewhere). The method is based on conformal transformation

$$z = w \cosh\left(\frac{\pi z_1}{w}\right), \quad (\text{B1})$$

which maps complex plane $z_1 = x_1 + iy_1$ into the complex plane $z = x + iy$ of our problem. Slit geometry in coordinates (x, y) corresponds to strip geometry in (x_1, y_1) coordinates: $0 < y_1 < w$, $-\infty < x_1 < \infty$. The Stokes equation, Eq. (4), describing flow of the incompressible fluid with $(\nabla \cdot \mathbf{v}) = 0$, dramatically simplifies in the new coordinates:

$$\frac{\partial \mathcal{F}}{\partial \bar{z}_1} = 0, \quad (\text{B2})$$

where complex potential is introduced

$$\mathcal{F} = \frac{\pi^2}{J} \omega + i \frac{eN}{\eta} \phi, \quad (\text{B3})$$

with ϕ for the electrical potential, and ω for the vorticity of the field $\mathbf{u} = \pi^{-1} \sqrt{J} \mathbf{v}_1$. Here, \mathbf{v}_1 is the velocity field in new coordinates and

$$J = \det(\partial x_\alpha / \partial x_{1\beta}) = \pi^2 \sinh(\pi z_1/w) \sinh(\pi \bar{z}_1/w)$$

is the Jacobian of the map. Any function $\mathcal{F} = \mathcal{F}(z_1)$ of a complex variable z_1 solves Eq. (B2). The imaginary part of this function yields the electrical potential, while the real part gives the vorticity up to the known factor J/π^2 .

In order to find velocity profiles starting from a given function $\mathcal{F}(z_1)$, one has to find stream function ψ of the field \mathbf{u} by solving equation $\omega = \Delta_1 \psi$. The solution depends on a certain function $A(z_1)$ that should be found from the boundary conditions.

Let us give several examples of solutions corresponding to the fixed potential drop between $y = -\infty$ and $y = \infty$, and obeying both no-slip and no-stress boundary conditions. For simplicity, we use below the units where the slit size and dimensionless voltage drop across the system are equal to unity: $w = 1$, and $\text{Im}\mathcal{F}(x, \infty) = -\text{Im}\mathcal{F}(x, -\infty) = 1/2$. The regular solution, discussed in the main body of the text corresponds to

$$\mathcal{F}^{(1)}(z_1) = -(i/2) \coth(\pi z_1/w). \quad (\text{B4})$$

This solution gives a regular distribution of the velocity in the slit:

$$v_y^{(1)}(x) = \frac{1}{4\pi} \sqrt{1-x^2}. \quad (\text{B5})$$

The same fixed voltage drop can also be reproduced by complex potential

$$\mathcal{F}^{(n)}(z_1) = -(i/2) \coth^n(\pi z_1/w)$$

with any positive integer n . It turns out that solutions with $n \geq 3$ are characterized by non-integrable vorticity and thus cannot be captured by the Keldysh-Sedov formula from Appendix A. For example, for $n = 3$ we have

$$v_y^{(3)} = \frac{1}{4\pi} \left(\sqrt{1-x^2} + \frac{1}{\sqrt{1-x^2}} \right).$$

We see that $v_y^{(3)}$ has integrable singularity at the slit edges. Hence, both $n = 1$ and $n = 3$ cases correspond to a finite current through the slit. Both these solutions are captured by method developed in the main text and can be obtained from Eqs. (32) and (27). At the same time, the solution with $n = 3$ yields infinite dissipation and should be discarded.

The solution corresponding to $n = 5$ has non-integrable velocity distribution inside the slit. In this case, we have

$$v_y^{(5)} = \frac{1}{4\pi} \left[\sqrt{1-x^2} + \frac{2}{\sqrt{1-x^2}} - \frac{1}{3(1-x^2)^{3/2}} \right].$$

This solution has strong singularity at the slit edge and, therefore, cannot be obtained within the integral-equation method used in the main body of the paper. Needless to say, the total dissipated power for this solution is divergent.

Appendix C: Solution with the partial-slip boundary condition: Finite slit vs. point source

In the main text, we have obtained a solution that satisfies both the no-slip (1) and no-stress (2) boundary

conditions. This solution is however does not coincide with solution in Ref. [48], where the point-source solution from Ref. [44] was invoked for deriving the velocity profile in the finite-slit geometry with the no-stress boundary condition. In this Appendix, we explicitly show why the solution for $w \equiv 0$ is inadequate for finding the velocity profile for a finite slit $w > 0$.

We will follow the derivation of Ref. [44] and require the velocity profile to satisfy (i) the ‘‘partial-slip’’ boundary condition Eq. (3) at barriers (i.e., $y = 0$ for $|x| > w$), and (ii) zero v_x in the slit (i.e., $y = 0$ for $|x| < w$). Rewriting these conditions through the stream function $\psi(x, y)|_{y=0}$, we have

$$\begin{cases} \frac{\partial \psi}{\partial y} = \lambda \frac{\partial^2 \psi}{\partial y^2}, & (y = 0, |x| \geq w), \\ \frac{\partial \psi}{\partial y} = 0, & (y = 0, |x| < w). \end{cases} \quad (\text{C1})$$

We can cast Eq. (C1) in terms of the Fourier transformed stream function $\tilde{\psi}(k, y)$, leading to

$$\begin{aligned} \frac{\partial \tilde{\psi}(k, y)}{\partial y} &= \lambda \frac{\partial^2 \tilde{\psi}(k, y)}{\partial y^2} \\ &- \frac{\lambda}{\pi} \int dk_1 \frac{\sin[(k - k_1)w]}{k - k_1} \frac{\partial^2 \tilde{\psi}(k_1, y)}{\partial y^2} \Big|_{y=0}. \end{aligned} \quad (\text{C2})$$

Substituting the general form of the solution, Eq. (E3), into Eq. (C2) we arrive at

$$\begin{aligned} &|k|c_1(k) - c_2(k) + \lambda[k^2c_1(k) - 2|k|c_2(k)] \\ &= \frac{\lambda}{\pi} \int \frac{dk_1}{k - k_1} \sin[(k - k_1)w][k_1^2c_1(k_1) - 2|k_1|c_2(k_1)]. \end{aligned} \quad (\text{C3})$$

By setting $w \equiv 0$ in Eq. (C3), we reproduce the relation from Ref. [44] (see Sec. II of its Supplementary Material):

$$c_2(k) = \frac{|k| + \lambda k^2}{1 + 2|k|\lambda} c_1(k). \quad (\text{C4})$$

Note that this relation is different from

$$c_2(k) = |k|c_1(k), \quad (\text{C5})$$

which corresponds to $v_x(x, 0) = 0$ at the wall (although they become equivalent for $\lambda = 0$). This, in particular, means that the asymptotic velocity profile at $r \rightarrow \infty$ is different for the two solutions, if $\lambda \neq 0$. For example, in the limit $\lambda \rightarrow \infty$, referred to as the no-stress case in Ref. [44], one obtains $c_2(k) = |k|c_1(k)/2$ from Eq. (C4). This difference in the factor of two is exactly the one that determines the difference between $\mathcal{C} = w^2$ in our solution and $\mathcal{C} = 2w^2$ in Ref. [48]. Indeed, Ref. [48] used the large- r asymptotics of the ‘‘point-source’’ solution (C4) to fix the constant \mathcal{C} for the no-stress boundary conditions. Finally, note that the finite- λ solution in Eq. (C4) is not provided by our general method, which leads to

Eq. (35), because it has non-integrable divergence of velocity $v_x \propto 1/x$ at $x \rightarrow 0$. Moreover, it generates divergent dissipation.

On a technical level, the reason behind this difference is that the kernel in the last (integral) term in Eq. (C3) acts as an effective delta-function for a broad class of integrated functions. In particular, it holds for any continuous velocity profile $v_y(x, y = 0)$ in our geometry that

$$\frac{1}{\pi} \int \frac{dk_1}{k - k_1} \sin[(k - k_1)w] k_1^2 c_1(k_1) = k^2 c_1(k), \quad (\text{C6})$$

and similarly for the term with $c_2(k)$ in Eq. (C3). This contribution to Eq. (C3) is, however, absent in if one sets $w \equiv 0$ before performing the integration over k_1 , thus completely disregarding the integral term. With Eq. (C6), the λ -dependent terms on both sides of Eq. (C3) cancel. We then immediately see that our solution (C5) with $v_x(x, 0) = 0$, which was originally obtained for the no-stress condition (2), is a valid solution for arbitrary λ . Representing the no-stress solution for a finite-slit problem ($w > 0$) through the point-source solution (C4) from Ref. [44] with $\lambda \rightarrow \infty$, as was done in Ref. [48], is thus not justified.

Appendix D: Work of the electric field

In the main text we have shown that with our solution the total viscosity-induced dissipation is equal to the work of the electric field. The corresponding resistance equals to that obtained by the resistance definition [5] for the no-slip boundary conditions. In this appendix, we consider the work of the electric field obtained with the choice $\mathcal{C} = 2w^2$ [48] for the velocity profile (11).

As the starter, electric field of our case agrees with that of Ref. [48]: only the velocity profiles are different. As we have already evaluated the work of the electric field of our case, in this appendix we only need to figure out the extra work induced by the velocity difference between our solution and that of Ref. [48]. The local extra work equals

$$Ne\delta\mathbf{v} \cdot \nabla\phi = -i \left(\delta\bar{u} \frac{\partial}{\partial z} - \delta u \frac{\partial}{\partial \bar{z}} \right) ne\phi, \quad (\text{D1})$$

where $\delta\mathbf{v}$ refers to the difference in velocity between the solution of Ref. [48] and that of the current paper, and $\delta u = \delta v_y + i\delta v_x$.

The total difference of the work done by the electric field in the bulk of the sample is given by

$$\begin{aligned} &-i \iint dx dy \left(\delta\bar{u} \frac{\partial}{\partial z} - \delta u \frac{\partial}{\partial \bar{z}} \right) ne\phi \\ &= \iint d\theta dr \frac{e^2 n^2 V^2}{16\eta} \frac{w^2 (w^2 - r^2 \cos 2\theta)}{[r^4 + w^4 - 2w^2 r^2 \cos(2\theta)]^{3/2}} \quad (\text{D2}) \\ &= \frac{\pi}{16} \frac{(eNVw)^2}{\eta}, \end{aligned}$$

which is twice as that of Eq. (22) of the superballistic case. Using this result, with the velocity profile of Ref. [48], the obtained resistance equals to

$$G_{2w^2} = \frac{3}{2}G_{\text{no-slip}}, \quad (\text{D3})$$

if evaluated by the total work done by the electric field in the bulk of the sample, where $G_{\text{no-slip}} = 1/R_{\text{no-slip}}$ is the superballistic conductance calculated in Ref. [5] for no-slip boundary conditions [see Eq. (23) of Sec. III]. This result, however, disagrees with the conductance obtained in Ref. [48] via the definition of the resistance $R = V/I$, where $G_{2w^2} = 2G_{\text{no-slip}}$ instead. Thus, for the velocity profile (11) with $C = 2w^2$, the resistances obtained by the three different methods (V^2/\mathcal{P} , V/I , and V^2/W) introduced in Sec. III are all different. This should be contrasted with the results of Sec. III for the finite-dissipation profile with $C = w^2$, for which all these three methods consistently yield the same resistance.

Appendix E: Derivation of the kernels for the integral equations

To obtain the kernels in Eq. (28), we apply a standard two-dimensional hydrodynamic technique and introduce the stream function $\psi(x, y)$, such that

$$v_x = \frac{\partial\psi}{\partial y}, \quad v_y = -\frac{\partial\psi}{\partial x}. \quad (\text{E1})$$

The Laplace equation $\Delta\omega = 0$ is then equivalent to the biharmonic equation

$$\Delta^2\psi = 0.$$

The Fourier transform with

$$\tilde{\psi}(k, y) = \int \psi(x, y)e^{-ikx} dx$$

leads us to the equation

$$\frac{\partial^4\tilde{\psi}(k, y)}{\partial y^4} - 2k^2\frac{\partial^2\tilde{\psi}(k, y)}{\partial y^2} + k^4\tilde{\psi}(k, y) = 0. \quad (\text{E2})$$

Since we are looking for the solution in the upper half-plane, we should keep only the partial solutions for which $\tilde{\psi}(k, y) \rightarrow 0$ when $y \rightarrow \infty$. Hence

$$\begin{aligned} \tilde{\psi}(k, y) &= c_1 e^{-|k|y} + c_2 y e^{-|k|y}, \\ \tilde{v}_x(k, y) &= -|k|c_1 e^{-|k|y} + (1 - |k|y)c_2 e^{-|k|y}, \\ \tilde{v}_y(k, y) &= -ik \left(c_1 e^{-|k|y} + c_2 y e^{-|k|y} \right). \end{aligned} \quad (\text{E3})$$

Here \tilde{v}_x, \tilde{v}_y denote the Fourier transforms of velocities

$$\begin{aligned} \tilde{v}_x(k, y) &= \int v_x(x, y)e^{-ikx} dx, \\ \tilde{v}_y(k, y) &= \int v_y(x, y)e^{-ikx} dx. \end{aligned}$$

It is now easy to express c_1 and c_2 through $\tilde{v}_x(k, 0)$ and $\tilde{v}_y(k, 0)$:

$$\begin{aligned} c_1 &= i \frac{\tilde{v}_y(k, 0)}{k} \\ c_2 &= \tilde{v}_x(k, 0) + \tilde{v}_y(k, 0) \frac{i|k|}{k} \end{aligned} \quad (\text{E4})$$

Expressing then $\tilde{v}_x(k, y)$ and $\tilde{v}_y(k, y)$ through $\tilde{v}_x(k, 0)$ and $\tilde{v}_y(k, 0)$, and performing the inverse Fourier transformation, we obtain

$$\begin{aligned} \vec{K}_1(x - x', y) &= \int \frac{dk}{2\pi} e^{-|k|y + ik(x-x')} \begin{pmatrix} 1 - |k|y \\ -iky \end{pmatrix}, \\ \vec{K}_2(x - x', y) &= \int \frac{dk}{2\pi} e^{-|k|y + ik(x-x')} \begin{pmatrix} -iky \\ 1 + |k|y \end{pmatrix}, \end{aligned} \quad (\text{E5})$$

which yields Eq. (28) of the main text.

Appendix F: Finding velocity on the walls through Chebyshev polynomials

In this Appendix, we demonstrate the uniqueness of the non-divergent solution

$$v_x(|x| > 1, y = 0) = 0$$

for the arbitrary λ boundary condition (3) with a finite λ . This is done by using an expansion of the velocity in Chebyshev polynomials (cf. Ref. [48]). It is possible to rewrite the equation for v_x using the new variable $\alpha = w/x$ in the following form:

$$v_x(\alpha, 0) = \frac{4\lambda\alpha^2}{\pi w} \frac{\partial}{\partial\alpha} \int_{-1}^1 \frac{1}{\alpha' - \alpha} v_x(\alpha', 0) d\alpha'. \quad (\text{F1})$$

If $v_x(\alpha)/\sqrt{1 - \alpha^2}$ is integrable inside the slit, we can expand the velocity $v_x(\alpha, 0)$ in the series:

$$v_x(\alpha, 0) = \sqrt{1 - \alpha^2} \sum_{n=0}^{\infty} C_n U_{2n+1}(\alpha). \quad (\text{F2})$$

Here $U_n(x)$ is the Chebyshev polynomial of the second kind, which satisfies the following relations:

$$\begin{aligned} \int_{-1}^1 \frac{\sqrt{1 - x^2} U_n(x)}{x' - x} dx' &= -\pi T_{n+1}(x), \\ \frac{\partial T_n(x)}{\partial x} &= n U_{n-1}(x), \end{aligned} \quad (\text{F3})$$

where $T_n(x)$ is the Chebyshev polynomial of the first kind. From the first line of (F2) we get

$$\sum_{n=0}^{\infty} \left[\sqrt{1 - \alpha^2} + \frac{8\lambda\alpha^2}{w} (n+1) \right] C_n U_{2n+1}(\alpha) = 0. \quad (\text{F4})$$

Using the definition of Chebyshev polynomials through trigonometric functions,

$$U_n(\alpha) = \frac{\sin[(n+1)\theta]}{\sin(\theta)}, \quad \alpha = \cos(\theta), \quad \theta \in [0, \pi], \quad (\text{F5})$$

we arrive at

$$\begin{aligned} & \sum_{n=0}^{\infty} C_n \left\{ \cos(2n+1)\theta - \cos(2n+3)\theta - \right. \\ & \left. - \frac{8\lambda(n+1)}{w} \sin 2(n+1)\theta - \frac{4\lambda(n+1)}{w} [\cos 2n\theta \right. \\ & \left. - \cos 2(n+2)\theta] \right\} = 0 \end{aligned} \quad (\text{F6})$$

For natural m and n , we have

$$\begin{aligned} \int_0^\pi \cos(nx) \cos(mx) dx &= \frac{\pi}{2} \delta_{m,n} \text{ (or } \pi \delta_{m,0} \text{ for } n=0), \\ \int_0^\pi \cos(nx) \sin(mx) dx &= \frac{[(-1)^{n+m} - 1]n}{m^2 - n^2}. \end{aligned} \quad (\text{F7})$$

We can multiple Eq. (F6) by $\cos(m\theta)$ and integrate it over θ with limits from 0 to π .

By using even m , we get

$$\begin{aligned} \left(\frac{m}{2} + 1\right) C_{\frac{m}{2}} &= \left(\frac{m}{2} + 3\right) C_{\frac{m}{2}+2}, \\ C_0 &= 0. \end{aligned} \quad (\text{F8})$$

For odd values of m , we obtain

$$\frac{\pi}{2} \left(C_{\frac{m-1}{2}} - C_{\frac{m-1}{2}-1} \right) + \frac{32\lambda}{w} \sum_{n=0}^{\infty} C_n \frac{(n+1)^2}{4(n+1)^2 - m^2} = 0. \quad (\text{F9})$$

Since m could be any natural number, we can safely establish the following relations for any integer k and for any odd m :

$$\begin{aligned} C_{k+2} &= \frac{k+1}{k+3} C_k, \\ C_{2k} &= 0, \quad C_{1+2k} = \frac{C_1}{k+1}, \\ \left(\frac{\pm\pi}{m \pm 1} + \frac{128\lambda}{w} \sum_{k=0}^{\infty} \frac{(k+1)}{16(k+1)^2 - m^2} \right) C_1 &= 0. \end{aligned} \quad (\text{F10})$$

Here the sign is $+$ if $(m-1)/2$ is even and $-$ if it is odd. From the divergence of the sum in the last line of Eq. (F10) we can conclude that the only meaningful solution has $C_1 = 0$ and, as follows from the second line of (F10), $C_n = 0$ for all n . Therefore $v_x(x, 0) = 0$ on the walls.

We should note here, that the Chebyshev polynomials expansion $f(x) = \sum_n C_n U_n(x)$ works only for functions with a finite integral $\int_{-1}^1 f(x) dx$. If we have a divergent, but integrable solution for v_x , which diverges as $1/\sqrt{1-\alpha^2}$ or stronger near the endpoints $\alpha = \pm 1$, then we cannot expand it in the way we did in Eq. (F2). Strictly speaking, there could exist nontrivial integrable divergent solutions for $v_x(x, 0)$ with the sign changes on the wall.

-
- [1] B. N. Narozhny, I. V. Gornyi, A. D. Mirlin, and J. Schmalian, *Hydrodynamic approach to electronic transport in graphene*, *Annalen der Physik* **529**, 1700043 (2017).
- [2] A. Lucas and K. C. Fong, *Hydrodynamics of electrons in graphene*, *J. Phys: Condens. Matter* **30**, 053001 (2018).
- [3] B. N. Narozhny, *Electronic hydrodynamics in graphene*, *Annals of Physics* **411**, 167979 (2019).
- [4] M. Polini and A. K. Geim, *Viscous electron fluids*, *Physics Today* **73**, 28 (2020).
- [5] H. Guo, E. Ilseven, G. Falkovich, and L. S. Levitov, *Higher-than-ballistic conduction of viscous electron flows*, *Proceedings of the National Academy of Sciences* **114**, 3068 (2017).
- [6] M. Shavit, A. Shtytov, and G. Falkovich, *Freely flowing currents and electric field expulsion in viscous electronics*, *Phys. Rev. Lett.* **123**, 026801 (2019).
- [7] D. A. Bandurin, I. Torre, R. K. Kumar, M. Ben Shalom, A. Tomadin, A. Principi, G. H. Auton, E. Khestanova, K. S. Novoselov, I. V. Grigorieva, L. A. Ponomarenko, A. K. Geim, and M. Polini, *Negative local resistance caused by viscous electron backflow in graphene*, *Science* **351**, 1055 (2016).
- [8] J. Crossno, J. K. Shi, K. Wang, X. Liu, A. Harzheim, A. Lucas, S. Sachdev, P. Kim, T. Taniguchi, K. Watanabe, T. A. Ohki, and K. C. Fong, *Observation of the dirac fluid and the breakdown of the Wiedemann-Franz law in graphene*, *Science* **351**, 1058 (2016).
- [9] P. J. W. Moll, P. Kushwaha, N. Nandi, B. Schmidt, and A. P. Mackenzie, *Evidence for hydrodynamic electron flow in PdCoO₂*, *Science* **351**, 1061 (2016).
- [10] F. Ghahari, H.-Y. Xie, T. Taniguchi, K. Watanabe, M. S. Foster, and P. Kim, *Enhanced thermoelectric power in graphene: Violation of the Mott relation by inelastic scattering*, *Phys. Rev. Lett.* **116**, 136802 (2016).
- [11] R. Krishna Kumar, D. A. Bandurin, F. M. D. Pellegrino, Y. Cao, A. Principi, H. Guo, G. H. Auton, M. Ben Shalom, L. A. Ponomarenko, G. Falkovich, K. Watanabe, T. Taniguchi, I. V. Grigorieva, L. S. Levitov, M. Polini, and A. K. Geim, *Superballistic flow of viscous electron fluid through graphene constrictions*, *Nature Physics* **13**, 1182 (2017).
- [12] D. A. Bandurin, A. V. Shtytov, L. S. Levitov, R. K. Kumar, A. I. Berdyugin, M. Ben Shalom, I. V. Grigorieva, A. K. Geim, and G. Falkovich, *Fluidity onset in graphene*, *Nature Communications* **9**, 4533 (2018).
- [13] B. A. Braem, F. M. D. Pellegrino, A. Principi, M. Rösli, C. Gold, S. Hannel, J. V. Koski, M. Berl, W. Dietsche,

- W. Wegscheider, M. Polini, T. Ihn, and K. Ensslin, *Scanning gate microscopy in a viscous electron fluid*, *Phys. Rev. B* **98**, 241304 (2018).
- [14] A. Jaoui, B. Fauqué, C. W. Rischau, A. Subedi, C. Fu, J. Gooth, N. Kumar, V. Süß, D. L. Maslov, C. Felser, and K. Behnia, *Departure from the Wiedemann–Franz law in WP2 driven by mismatch in T-square resistivity prefactors*, *npj Quantum Materials* **3**, 64 (2018).
- [15] A. D. Levin, G. M. Gusev, E. V. Levinson, Z. D. Kvon, and A. K. Bakarov, *Vorticity-induced negative nonlocal resistance in a viscous two-dimensional electron system*, *Phys. Rev. B* **97**, 245308 (2018).
- [16] J. Gooth, F. Menges, N. Kumar, V. Süß, C. Shekhar, Y. Sun, U. Drechsler, R. Zierold, C. Felser, and B. Gotsmann, *Thermal and electrical signatures of a hydrodynamic electron fluid in tungsten diphosphide*, *Nature Communications* **9**, 4093 (2018).
- [17] A. I. Berdyugin, S. G. Xu, F. M. D. Pellegrino, R. Krishna Kumar, A. Principi, I. Torre, M. Ben Shalom, T. Taniguchi, K. Watanabe, I. V. Grigorieva, M. Polini, A. K. Geim, and D. A. Bandurin, *Measuring Hall viscosity of graphene’s electron fluid*, *Science* **364**, 162 (2019).
- [18] P. Gallagher, C.-S. Yang, T. Lyu, F. Tian, R. Kou, H. Zhang, K. Watanabe, T. Taniguchi, and F. Wang, *Quantum-critical conductivity of the Dirac fluid in graphene*, *Science* **364**, 158 (2019).
- [19] J. A. Sulpizio, L. Ella, A. Rozen, J. Birkbeck, D. J. Perello, D. Dutta, M. Ben-Shalom, T. Taniguchi, K. Watanabe, T. Holder, R. Queiroz, A. Principi, A. Stern, T. Scaffidi, A. K. Geim, and S. Ilani, *Visualizing Poiseuille flow of hydrodynamic electrons*, *Nature* **576**, 75 (2019).
- [20] L. Ella, A. Rozen, J. Birkbeck, M. Ben-Shalom, D. Perello, J. Zultak, T. Taniguchi, K. Watanabe, A. K. Geim, S. Ilani, and J. A. Sulpizio, *Simultaneous voltage and current density imaging of flowing electrons in two dimensions*, *Nature Nanotechnology* **14**, 480 (2019).
- [21] M. J. H. Ku, T. X. Zhou, Q. Li, Y. J. Shin, J. K. Shi, C. Burch, L. E. Anderson, A. T. Pierce, Y. Xie, A. Hamo, U. Vool, H. Zhang, F. Casola, T. Taniguchi, K. Watanabe, M. M. Fogler, P. Kim, A. Yacoby, and R. L. Walsworth, *Imaging viscous flow of the Dirac fluid in graphene*, *Nature* **583**, 537 (2020).
- [22] O. E. Raichev, G. M. Gusev, A. D. Levin, and A. K. Bakarov, *Manifestations of classical size effect and electronic viscosity in the magnetoresistance of narrow two-dimensional conductors: Theory and experiment*, *Phys. Rev. B* **101**, 235314 (2020).
- [23] G. M. Gusev, A. S. Jaroshevich, A. D. Levin, Z. D. Kvon, and A. K. Bakarov, *Stokes flow around an obstacle in viscous two-dimensional electron liquid*, *Scientific Reports* **10**, 7860 (2020).
- [24] U. Vool, A. Hamo, G. Varnavides, Y. Wang, T. X. Zhou, N. Kumar, Y. Dovzhenko, Z. Qiu, C. A. C. Garcia, A. T. Pierce, J. Gooth, P. Anikeeva, C. Felser, P. Narang, and A. Yacoby, *Imaging phonon-mediated hydrodynamic flow in WTe₂ with cryogenic quantum magnetometry* (2020), [arXiv:2009.04477 \[cond-mat.mes-hall\]](https://arxiv.org/abs/2009.04477).
- [25] J. Geurs, Y. Kim, K. Watanabe, T. Taniguchi, P. Moon, and J. H. Smet, *Rectification by hydrodynamic flow in an encapsulated graphene Tesla valve* (2020), [arXiv:2008.04862 \[cond-mat.mes-hall\]](https://arxiv.org/abs/2008.04862).
- [26] M. Kim, S. G. Xu, A. I. Berdyugin, A. Principi, S. Slizovskiy, N. Xin, P. Kumaravadivel, W. Kuang, M. Hamer, R. Krishna Kumar, R. V. Gorbachev, K. Watanabe, T. Taniguchi, I. V. Grigorieva, V. I. Fal’ko, M. Polini, and A. K. Geim, *Control of electron-electron interaction in graphene by proximity screening*, *Nature Communications* **11**, 2339 (2020).
- [27] A. Jenkins, S. Baumann, H. L. Zhou, S. A. Meynell, D. Y. Yang, K. Watanabe, T. Taniguchi, A. Lucas, A. F. Young, and A. C. B. Jayich, (2020), [arXiv:2002.05065 \[cond-mat.mes-hall\]](https://arxiv.org/abs/2002.05065).
- [28] A. Gupta, J. J. Heremans, G. Kataria, M. Chandra, S. Fallahi, G. C. Gardner, and M. J. Manfra, *Hydrodynamic and ballistic transport over large length scales in GaAs/AlGaAs*, *Phys. Rev. Lett.* **126**, 076803 (2021).
- [29] G. M. Gusev, A. S. Jaroshevich, A. D. Levin, Z. D. Kvon, and A. K. Bakarov, *Viscous magnetotransport and Gurzhi effect in bilayer electron system*, *Phys. Rev. B* **103**, 075303 (2021).
- [30] Y. Zhang and M. S. Shur, *Collision dominated, ballistic, and viscous regimes of terahertz plasmonic detection by graphene*, *Journal of Applied Physics* **129**, 053102 (2021).
- [31] A. Jaoui, B. Fauqué, and K. Behnia, *Thermal resistivity and hydrodynamics of the degenerate electron fluid in antimony*, *Nature Communications* **12**, 195 (2021).
- [32] Z. J. Krebs, W. A. Behn, S. Li, K. J. Smith, K. Watanabe, T. Taniguchi, A. Levchenko, and V. W. Brar, *Imaging the breaking of electrostatic dams in graphene for ballistic and viscous fluids* (2021), [arXiv:2106.07212 \[cond-mat.mes-hall\]](https://arxiv.org/abs/2106.07212).
- [33] C. Kumar, J. Birkbeck, J. A. Sulpizio, D. J. Perello, T. Taniguchi, K. Watanabe, O. Reuven, T. Scaffidi, A. Stern, A. K. Geim, and S. Ilani, *Imaging hydrodynamic electrons flowing without Landauer-Sharvin resistance* (2021), [arXiv:2111.06412 \[cond-mat.mes-hall\]](https://arxiv.org/abs/2111.06412).
- [34] A. Aharon-Steinberg, T. Völkl, A. Kaplan, A. K. Pariari, I. Roy, T. Holder, Y. Wolf, A. Y. Meltzer, Y. Myasoedov, M. E. Huber, B. Yan, G. Falkovich, L. S. Levitov, M. Hücker, and E. Zeldov, *Direct observation of vortices in an electron fluid*, *Nature* **607**, 74 (2022).
- [35] A. Finkler, Y. Segev, Y. Myasoedov, M. L. Rappaport, L. Ne’eman, D. Vasyukov, E. Zeldov, M. E. Huber, J. Martin, and A. Yacoby, *Self-aligned nanoscale SQUID on a tip*, *Nano Letters* **10**, 1046 (2010).
- [36] D. Vasyukov, Y. Anahory, L. Embon, D. Halbertal, J. Cuppens, L. Neeman, A. Finkler, Y. Segev, Y. Myasoedov, M. L. Rappaport, M. E. Huber, and E. Zeldov, *A scanning superconducting quantum interference device with single electron spin sensitivity*, *Nature Nanotechnology* **8**, 639 EP (2013).
- [37] D. Halbertal, J. Cuppens, M. B. Shalom, L. Embon, N. Shadmi, Y. Anahory, H. R. Naren, J. Sarkar, A. Uri, Y. Ronen, Y. Myasoedov, L. S. Levitov, E. Joselevich, A. K. Geim, and E. Zeldov, *Nanoscale thermal imaging of dissipation in quantum systems*, *Nature* **539**, 407 (2016).
- [38] D. Halbertal, M. Ben Shalom, A. Uri, K. Bagani, A. Y. Meltzer, I. Marcus, Y. Myasoedov, J. Birkbeck, L. S. Levitov, A. K. Geim, and E. Zeldov, *Imaging resonant dissipation from individual atomic defects in graphene*, *Science* **358**, 1303 (2017).
- [39] A. Marguerite, J. Birkbeck, A. Aharon-Steinberg, D. Halbertal, K. Bagani, I. Marcus, Y. Myasoedov, A. K. Geim, D. J. Perello, and E. Zeldov, *Imaging work and dissipation in the quantum hall state in graphene*, *Nature* **575**, 628 (2019).

- [40] A. Uri, Y. Kim, K. Bagani, C. K. Lewandowski, S. Grover, N. Auerbach, E. O. Lachman, Y. Myasoedov, T. Taniguchi, K. Watanabe, J. Smet, and E. Zeldov, *Nanoscale imaging of equilibrium quantum hall edge currents and of the magnetic monopole response in graphene*, *Nature Physics* **16**, 164 (2020).
- [41] Y. Anahory, H. R. Naren, E. O. Lachman, S. Buhbut Sinai, A. Uri, L. Embon, E. Yaakobi, Y. Myasoedov, M. E. Huber, R. Klajn, and E. Zeldov, *Squid-on-tip with single-electron spin sensitivity for high-field and ultra-low temperature nanomagnetic imaging*, *Nanoscale* **12**, 3174 (2020).
- [42] A. Aharon-Steinberg, A. Marguerite, D. J. Perello, K. Bagani, T. Holder, Y. Myasoedov, L. S. Levitov, A. K. Geim, and E. Zeldov, *Long-range nontopological edge currents in charge-neutral graphene*, *Nature* **593**, 528 (2021).
- [43] I. Torre, A. Tomadin, A. K. Geim, and M. Polini, *Non-local transport and the hydrodynamic shear viscosity in graphene*, *Phys. Rev. B* **92**, 165433 (2015).
- [44] G. Falkovich and L. Levitov, *Linking spatial distributions of potential and current in viscous electronics*, *Phys. Rev. Lett.* **119**, 066601 (2017).
- [45] J. C. Maxwell, *On stresses in rarified gases arising from inequalities of temperature*, *Phil. Trans. R. Soc.* **170**, 231–256 (1879).
- [46] E. I. Kiselev and J. Schmalian, *Boundary conditions of viscous electron flow*, *Phys. Rev. B* **99**, 035430 (2019).
- [47] M. Rokni and Y. Levinson, *Joule heat in point contacts*, *Phys. Rev. B* **52**, 1882 (1995).
- [48] S. S. Pershoguba, A. F. Young, and L. I. Glazman, *Current distribution in a slit connecting two graphene half planes*, *Phys. Rev. B* **102**, 125404 (2020).
- [49] S. Li, M. Khodas, and A. Levchenko, *Conformal maps of viscous electron flow in the Gurzhi crossover*, *Phys. Rev. B* **104**, 155305 (2021).
- [50] M. Qi and A. Lucas, *Distinguishing viscous, ballistic, and diffusive current flows in anisotropic metals*, *Phys. Rev. B* **104**, 195106 (2021).
- [51] M. Lavrentev and B. Shabat, *Methods of the theory of function of complex variable* (Nauka, Moscow, 1973).
- [52] H. Lamb, *Hydrodynamics* (Dover publications, New York, 1945).
- [53] Y.-M. Koh, *Vorticity and viscous dissipation in an incompressible flow*, *KSME Journal* **8**, 35–42 (1993).
- [54] A. Polyanin and A. Manzhirov, *Handbook of integral equations* (CRC Press LLC, Boca Raton, Florida, 1998).
- [55] L. Landau and E. Lifshitz, *Course of Theoretical Physics, Volume 6, Fluid Mechanics* (Pergamon Press, Oxford, 1987).
- [56] K. S. Tikhonov, I. V. Gornyi, V. Y. Kachorovskii, and A. D. Mirlin, *Asymmetry of nonlocal dissipation: From drift-diffusion to hydrodynamics*, *Phys. Rev. B* **100**, 205430 (2019).
- [57] G. Zhang, V. Kachorovskii, K. Tikhonov, and I. Gornyi, *Heating of inhomogeneous electron flow in the hydrodynamic regime*, *Phys. Rev. B* **104**, 075417 (2021).